J Fluoresc (2013) 23:761–766
DOI 10.1007/s10895-013-1195-9

ORIGINAL PAPER

A TDDFT Study on the Excited-State Intramolecular Proton Transfer (ESIPT): Excited-State Equilibrium Induced by Electron Density Swing

Mingzhen Zhang · Dapeng Yang · Baiping Ren · Dandan Wang

Received: 15 September 2012 / Accepted: 24 February 2013 / Published online: 15 March 2013

Abstract One important issue of current interest is the excited-state equilibrium for some ESITP dyes. However, so far, the information about the driving forces for excited-state equilibrium is very limited. In this work, the time-dependent density functional theory (TDDFT) method was employed to investigate the nature of the excited-state intramolecular proton transfer (ESIPT). The geometric structures, vibrational frequencies, frontier molecular orbitals (MOs) and the potential-energy curves for 1-hydroxy-11H-benzo[b]fluoren-11-one (HHBF) in the ground and the first singlet excited state were calculated. Analysis of the results shows that the intramolecular hydrogen bond of HHBF is strengthened from E to E*. Moreover, it is found that electron density swing between the proton acceptor and donor provides the driving forces for the forward and backward ESIPT, enabling the excited-state equilibrium to be established. Furthermore, we proposed that the photoexcitation and the interchange of position for electron-donating and electron-withdrawing groups are the main reasons for the electron density swing. The potential-energy curves suggest that the forward ESIPT and backward ESIPT may happen on the similar timescale, which is faster than the fluorescence decay of both E* and K* forms.

Keywords Excited state · Hydrogen bond · Proton transfer · ESIPT · TDDFT

M. Zhang · D. Yang · B. Ren · D. Wang
State Key Laboratory of Molecular Reaction Dynamics, Dalian Institute of Chemical Physics, Chinese Academy of Sciences, Dalian 116023, China

M. Zhang · D. Yang (✉) · B. Ren · D. Wang
Physics Laboratory, North China University of Water Resources and Electric Power, 36 Beihuan Road, Zhengzhou 450011, China
e-mail: yangdp_ncwu@126.com

Introduction

During the past decades, excited-state intramolecular proton transfer (ESIPT) has gained much attention because of its remarkable applications in the molecular probe, enzyme catalysis and luminescent material [1–17]. A great number of works have been performed to investigate its photophysical and chemical properties, aiming to develop the high performance materials [2–14, 16, 17].

The basic process of the ESIPT has been illustrated in a large number of literatures [18–29]. Herein, for the convenience of the latter discussion, the brief introduction of ESIPT is provided, as shown in Fig. 1. The ESIPT dyes exist as the enol form (E) in the ground state, forming the intramolecular hydrogen bonds. Upon the photoexcitation, ESIPT occurs at a high rate of speed, transforming the enol form (E*) to the keto tautomer (K*) in the excited state. Then the keto form (K*) in the excited state deactivates to the ground state (K). Finally, the keto form (K) is transformed to the enol form (E) in the ground state. Due to the drastic structural alternations, the tautomer (keto form) usually possesses different photophysical properties compared to the original species. Thus the ESIPT dyes can present the relative large Stokes shift, which is regarded as the most remarkable advantages of the ESIPT molecules.

Attempts exploiting ESIPT molecules as the white lighting materials have recently been a hot area of research [30, 31]. As we all know that the white luminescence is unusual because the luminophore can't give the emission covering a wide range of the visible spectrum [6]. In this case, mixing two or more luminophores showing the different emission colors together to get the white light emission seems to be feasible. In 2005, Park and co-workers designed a white lighting material containing two ESIPT fluorophores of SOX and DOX [32]. Upon the ESIPT process, these two fluorophores give the different emission wavelengths without overlap between the emission and the absorption. Thus by a specific concentration

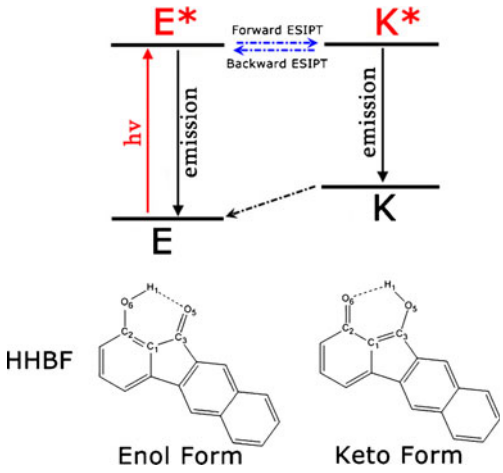

Fig. 1 Structures and atomic numbers for HHBF, and the corresponding ESIPT mechanism. *E* denotes the enol form in the ground state. *E** denotes the enol form in the first excited state. *K* denotes the keto form in the ground state. *K** denotes the keto form in the first excited state. The proton transfer from E* to K* is defined as forward ESIPT. The proton transfer from K* to E* is defined as backward ESIPT

proportion, they successfully got the white lighting system. Later in 2009, they linked two ESIPT fluorophores with the covalent bond, obtaining the concentration-independent white lighting material [5]. Furthermore, in 2010 year, Chou and co-workers developed another single ESIPT dye which shows the balanced enol- and keto emission simultaneously [6]. They investigated three ESIPT dyes and purposed that, for 7-hydroxy-2,3-dihydro-1H-inden-1-one [33], only the forward ESIPT happens. But for 1-hydroxy-9H-fluoren-9-one and 1-hydroxy-11H-benzo[b]fluoren-11-one (HHBF), both of forward and backward ESIPT happen, namely, they can get the excited-state equilibrium between the E* and K* form. Along with these unique features, HHBF amazingly gets the white light emission. However, so far, the reasons for its excited-state equilibrium are still unknown.

One important issue of current interest is the excited-state equilibrium for some ESITP dyes. In the past, based on the thermodynamic and kinetic analysis, two possible mechanisms were proposed to explain the appearance of two bands in steady-state emission spectra [34]. However, the information about the driving forces for excited-state equilibrium is very limited.

In the present work, HHBF (shown in Fig. 1) is employed to investigate its ESIPT properties, aiming to study the reasons for the excited state equilibrium. Firstly, by analyzing the absorption spectra, it is confirmed that the calculating methods selected in the present paper is relatively suitable for the theoretical study of the target system. Meanwhile, the comparisons of the emission spectra ensure the occurrence of ESIPT for the target system during the photoreaction processes. By studying the vibrational frequencies of the stretching vibrations of O6–H1 and C3=O5 involved in the hydrogen bond, the intramolecular hydrogen bonds are demonstrated to be strengthened upon the photoexcitation. Moreover, the results of the geometric structures of HHBF show the distinct decrease of the intramolecular hydrogen bond lengths from E to E*. Analyzing the frontier MOs for the enol form and keto form in the ground and the first excited state, we amazingly found that the electron density swing between the proton acceptor and donor provides the driving forces for the forward and the backward ESIPT, enabling the excited-state equilibrium to be established. And the reasons for electron density swing can be attributed to the photoexcitation and the interchange of position for the electron-donating group and the electron-withdrawing group. Finally, thermodynamics explanations for the excited-state equilibrium are also provided by studying the potential-energy curves.

Computational Details

All the electronic structure calculations were carried out using the Gaussian 09 program suite. All the geometry optimizations of HHBF in the ground and the first excited states were performed using density functional theory (DFT) and time-dependent density functional theory (TDDFT), respectively. The basis set 6-311+(2d,2p) and Becke's three-parameter hybrid exchange function with Lee–Yang–Parr gradient-corrected correlation functional (B3LYP) were employed for all the calculations [35–37]. Moreover, no constrains for symmetry, bonds, angles, or dihedral angles were employed in the geometry optimization calculations. In the view of the solvent effect, cyclohexane was used as solvent in the SCRF calculations using PCM throughout. All the local minima were confirmed by the absence of an imaginary mode in vibrational analysis calculations. Additionally, the potential-energy curves for HHBF in the ground and the first excited state were qualitatively scanned by constrained optimizations, fixing the intramolecular hydrogen bond distance at a serious of values.

Results and Discussion

In order to verify the applicability of the calculating methods, the excitation energies of the enol form (E) in the ground state and corresponding oscillation strengths of HHBF were calculated. For comparing to the experimental results intuitively, we integrate the data and draw the absorption spectra shown in Fig. 2. The corresponding experimental results are also shown using the blue lines. As we can clearly see that, for HHBF, the calculated absorption peak is 421.99 nm while the corresponding experimental absorption peak is 409.00 nm. It is obvious that the theoretical and experimental results show the high consistency. Accordingly, one can get the conclusions that DFT,

TDDFT and the corresponding basis set (6-311+2d,2p) are relatively suitable for the theoretical studies of the target system.

Experimentally, HHBF is found to consist of two emission wavelengths in the steady-state spectra, one of which shows the large Stocks shift compared to the absorption wavelength. However, whether this emission wavelength showing the large Stocks shift is caused by ESIPT is indeterminate. In other word, for HHBF, there is no direct evidence for the occurrence of ESIPT. In order to further study this issue, the emission spectra of the keto form (K*) in the first excited state are calculated and shown in Fig. 2. As is well known, if ESIPT happens during the photoreaction process, the experimental emission wavelength showing the large Stocks shift should correspond to the calculated emission wavelength of the keto form (K*) in the first excited state. As is seen in Fig. 2, the calculated emission wavelength is 603.14 nm while that of experiment is 621.00 nm. The calculated and the experimental results are in good agreement with each other. So this high degree of consistency directly supports the occurrence of ESIPT (Fig. 3).

The excited-state hydrogen bond plays a significant role in ESIPT process [38–48]. Thus, the study of hydrogen bonding dynamics in the excited state is the key to understand ESIPT. As is known, the vibrational frequencies of the stretching vibrations of O6–H1 and C3=O5 involved in the hydrogen bond can provide a clear-cut signature of excited-state hydrogen-bonding dynamics [42]. Zhao and co-workers proposed for the first time that the excited-state hydrogen bond strengthening can be induced by the redshifts of vibrational frequencies involved in the hydrogen bond [38–44]. In the present work, the IR spectra of HHBF were calculated and shown in Fig. 4. For HHBF, one can clearly see that the C3=O5 stretching band appears at 1712.14 cm^{-1} in the ground state (E). In the excited state (E*), the C3=O5 stretching band is redshifted to 1605.60 cm^{-1}. Meanwhile, the O6–H1

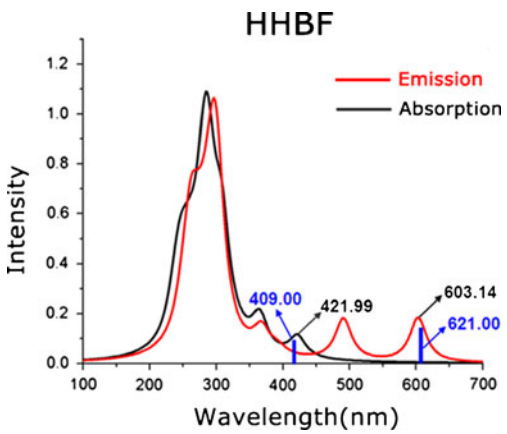

Fig. 2 Calculated absorption and emission spectra for HHBF. The *blue lines* show the corresponding results observed in experiment

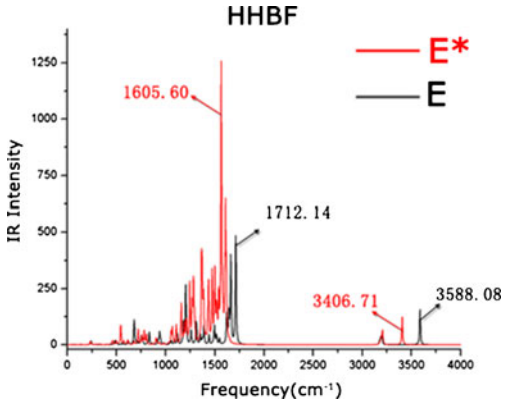

Fig. 3 The optimized geometric structures of enol and keto form for HHBF in the ground and the first singlet excited state together with the intramolecular hydrogen bond lengths. The corresponding planer structures are shown on the *right side*

stretching band appears at 3588.08 cm^{-1} in the ground state(E) and subsequently be redshifted to 3406.71 cm^{-1} in the excited state(E*). Based on the conclusions presented by Zhao mentioned above, the results of the IR spectra show obviously that, from E to E*, the intramolecular hydrogen bond of HHBF is strengthened.

The analysis of the geometric structures provides the further evidence for the strengthening of the intramolecular hydrogen bond. The optimized geometric structures of enol and keto form for HHBF in the ground and the first singlet excited state were obtained using DFT and TDDFT with the B3LYP functional and the 6-311g+(2d,2p) basis set, shown in Fig. 3 together with the corresponding hydrogen bond lengths. To evaluate the solvent effect, cyclohexane was

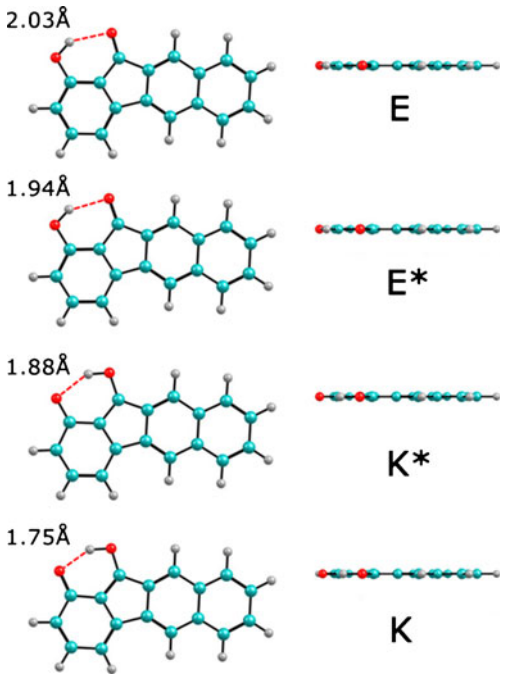

Fig. 4 Calculated IR spectra of HHBF for E (*black*) and E* (*red*)

used in the calculations according to PCM. The local minima only have real frequencies. The geometric structures in the vicinity of intramolecular hydrogen bonds are shown in Table 1. The corresponding atom numbers can be seen in Fig. 1. On the one hand, it is obvious that the molecular planarity is maintained perfectly for all the structures of HHBF, in other word, all the atoms of the molecules are consistently in the same plane during the whole photochemical process. On the other hand, from E to E*, we can see that the intramolecular hydrogen bond length decreases from 2.04 Å to 1.96 Å, whereas the other bond lengths don't change. As is well known, the ESIPT rate depends critically on the distance between the proton donor and acceptor, namely, on the length of intramolecular hydrogen bond. Consequently, there is no doubt that the decreases of intramolecular hydrogen bond lengths from E to E* is a very important positive factor for the forward ESIPT.

Frontier MOs analysis can directly provide insights into the nature of electronically excited states [49–54]. All the frontier molecular orbitals (MOs) of HHBF were calculated and shown in Fig. 5. From the TD-DFT results, it can be known that the first excited states of HHBF for both enol and keto form are a dominant $\pi\pi^*$-type transition from the highest occupied molecular orbital (HOMO) to the lowest unoccupied molecular orbital (LUMO). Accordingly, only the HOMOs and LUMOs for the enol and the keto form are shown in Fig. 5. Upon the photoexcitation, the electron density formerly located on the oxygen atom O6 decreases while that on the oxygen atom O5 increases, which indicates that the excitation from E to E* should involved intramolecular electron density transfer from O6 to O5. As a consequence, the proton acceptor (O5) is expected to be more basic, whereas the proton donor (O6) is more acid with respect to the ground state (E), driving the proton transfer from O6 to O5 (forward ESIPT). After the forward ESIPT, the electron density of the molecule is redistributed again. In particular, from E* to K*, the electron density located on O6 increases while that on O5 decrease, which shows the distinct intramolecular charge transfer from O5 to O6. This may provide the driving force for the proton transfer from O5 to O6 (backward ESIPT), enabling the excited-state equilibrium to be established. Therefore, based on the above discussions, it can be tentatively put forward that the electron density swing between the proton acceptor and donor provides the driving forces for the excited-state equilibrium.

Table 1 Calculated bond lengths L (Å), bond angles ∠(∘) and dihedral angles ψ(∘) of HHBF for the enol form in the ground (E) and the first singlet excited state (E*) as well as that for the keto form in the excited state (K*)

	E	E	K*
L H1–O5	2.03	1.94	0.99
L C2–O6	1.35	1.35	1.27
L O6–H1	0.98	0.98	1.88
L C3–O5	1.23	1.27	1.33
∠O6–H1–O5	143.4	147.4	146.6
∠C2–O6–H1	108.0	106.4	98.1
∠C3–O5–H1	94.3	94.1	104.6
ψC1–C2–O6–H1	0	0	0
ψC1–C3–O5–H1	0	0	0

The mechanism for the electron density swing can be illustrated in Fig. 6. As is shown in Fig. 6a, it is clear that the intramolecular electron density transfer from O6 to O5 is triggered by the photoexcitation. Subsequently, for E* in Fig. 6b, one can see that the hydroxyl is formed between O6 and H1 while carbonyl is formed between O5 and C3. Due to the forward ESIPT, the hydroxyl is formed between O5 and H1 while carbonyl is formed between O6 and C2 for K*. As we all know that, in conjugated system, the hydroxyl group is the electron-donating group and the carbonyl is the electron-withdrawing group. Consequently, the interchange of position for electron-donating group and electron-withdrawing group in the excited state will change the intramolecular electron density distribution, driving the intramolecular electron density transferring from O5 to O6. In general, the electron density swing is the result of both the photoexcitation and the interchange of position for the electron-donating group and the electron-withdrawing group.

The potential-energy curves of HHBF as a function of the O5–H1 bond length were calculated (shown in Fig. 7) to show the thermodynamic properties of ESIPT. Firstly, we can see that, in the ground states, the potential energy of HHBF for enol form (E) is much smaller than that for keto form (K). As a result, proton transfer from K to E is populated in the ground states. For the excited state, we can see that the forward ESIPT will cross an energy barrier (8.119 kcal/mol) while that for backward ESIPT is 3.751 kcal/mol. It is clear that the energy barriers of the forward and the backward ESIPT are in the same order of magnitude. Thus, it can be expected that the forward and the backward ESIPT may happen on the similar timescale, which is faster than the fluorescence decay of both E* and K* forms. This may lead to the rapidly established excited-state equilibrium.

Conclusion

In summary, we theoretically studied the nature of ESIPT for HHBF. Firstly, the comparisons of the absorption spectra confirm that the TDDFT, DFT and corresponding basis set 6-311+(2d,2p) are suitable for the theoretical studies of the target system. Besides, the comparisons of the emission

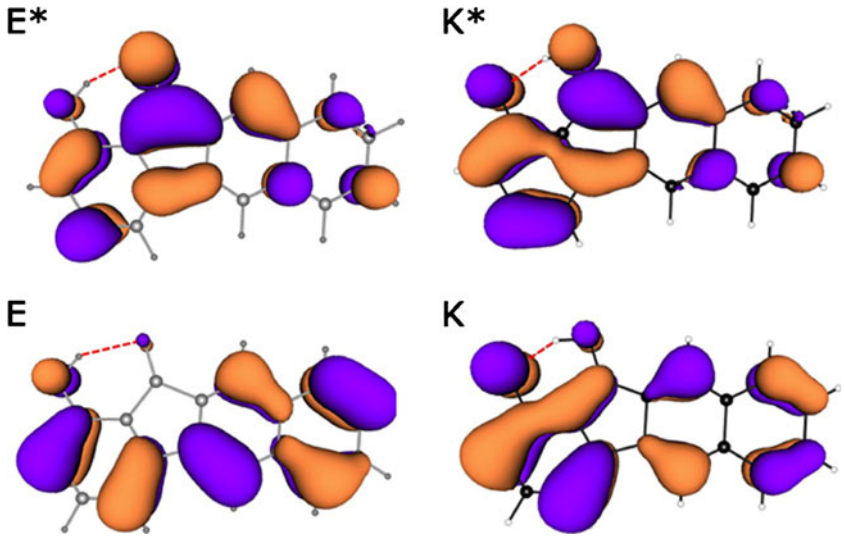

Fig. 5 The frontier molecular orbitals (MOs) of HHBF for E, E*, K and K*

spectra directly ensure the occurrence of ESIPT for the target system during the photoreaction processes.

Furthermore, by studying the vibrational frequencies of the stretching vibrations of O6–H1 and C3=O5 involved in the hydrogen bond, the intramolecular hydrogen bond is demonstrated to be strengthened upon the photoexcitation.

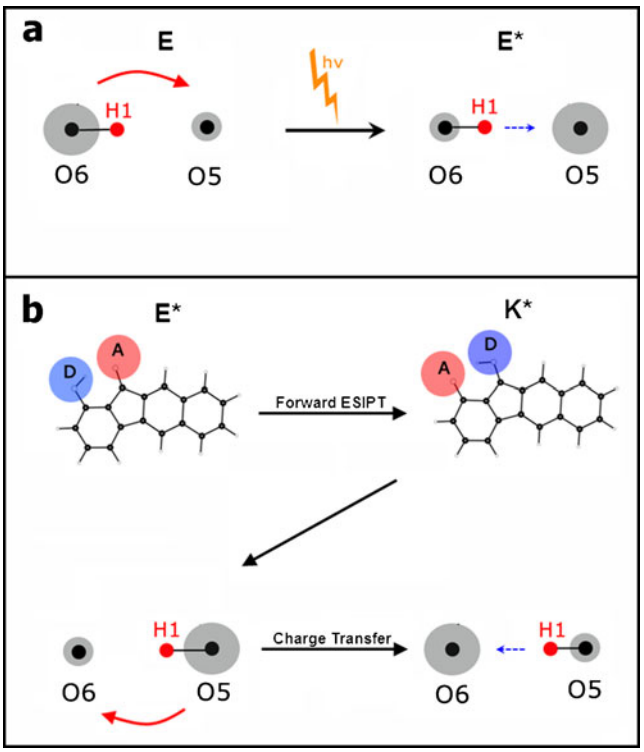

Fig. 6 **a** The schematic diagrams for the intramolecular electron density transfer from O6 to O5 drived by the photoexcitation. **b** *D* denotes the hydroxyl group (electron donative group). *A* denotes the carbonyl group (electron withdrawing group). The *red arrows* denotes the direction of the electron density transfer. Due to the forward ESIPT, D and A interchange with each other. Subsequently, the electron density transfers from O5 to O6

Meanwhile, analysis of the geometric structures clearly shows that the intramolecular hydrogen bond length is shortened upon the photoexcitation, which is regarded as a very important positive factor for forward ESIPT.

By analyzing the frontier MOs for the enol form and keto form in both ground and the excited state, we amazingly found that the electron density swing between the proton donor and proton acceptor provides the driving forces for the forward ESIPT and backward ESIPT, enabling the excited-state equilibrium to be established. And the reason for electron density swing can be attributed to the photoexcitation and the interchange of position for the electron donor and the electron withdrawing group.

Finally, the potential-energy curves of HHBF as a function of the O5–H1 bond length were calculated to show the thermodynamic properties of ESIPT It is found that the energy barriers of the forward and the backward ESIPT are in the same order of magnitude. As a result, it is deduced that the forward and the backward ESIPT may happen on the similar

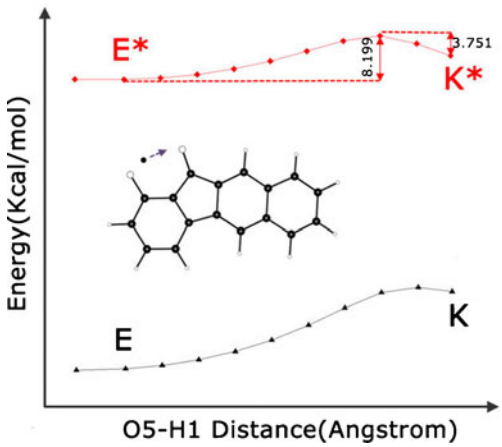

Fig. 7 Calculated potential-energy curves of HHBF as a function of the O5–H1 bond length in the ground and the first excited state

timescale, which is faster than the fluorescence decay of both E* and K* forms. This can be expected to be the thermodynamics explanations for the excited-state equilibrium.

References

1. Wu JS, Liu M, Ge JC, Zhang HY, Wang PE (2011) Chem Soc Rev 40:3493–3495
2. Fang C, Frontier RR, Tran R, Mathies RA (2009) Nature 462:201
3. Tanner C, Monca C, Leutwyler S (2003) Science 302:1736
4. Kwon JE, Park SY (2011) Adv Mater 23:3615–3642
5. Park S, Kwon JE, Seo J, Chung K, Park SY (2009) J Am Chem Soc 131:14043–14049
6. Tang KC, Chang MJ, Lin TY, Pan HA, Fang TC, Chen KY, Huang WY, Hsu YH, Chou PT (2011) J Am Chem Soc 133:17738–17745
7. Mutai T, Tomoda H, Ohkawa T, Yabe Y, Araki K (2008) Angew Chem Int Ed 47:9522–9524
8. Sakai K, Takahashi S, Kobayashi A, Akutagawa T, Nakamura T, Dosen M, Kata M, Nagashima U (2010) Dalton Trans 39:1989–1995
9. Lim CK, Seo J, Kim S, Kwon IC, Ahn CH, Park SY (2011) Dyes Pigments 90:284–289
10. Nah MK, Rho SG, Kim HK, Kang JG (2007) J Phys Chem A 11:11437–11443
11. Li X, Qian Y, Wang S, Li S, Yang G (2009) J Phys Chem C 113:3862–3868
12. Sun WH, Li S, Hu R, Qian Y, Wang S, Yang G (2009) J Phys Chem A 11:5888
13. Naama KL, Itay P, Erez Y, Rinat G, Doron S, Dan H (2012) J Phys Chem A 116:85–92
14. Wu F, Ma L, Zhang S, Geng Y, Lu J, Cheng X (2012) Chem Phys Lett 519:141–144
15. Park SY, Hyeok J, Hahkjoon K (2011) J Phys Chem C 115:24763
16. McCarthy A, Ruth AA (2011) Phys Chem Chem Phys 13:18661–18670
17. Ramprasad M, Bhattacharyya SP, Abhijit M (2011) J Phys Chem B 115:11840–11851
18. Hsieh CC, Chou PT, Shih WC, Chuang WT, Chung MW, Lee J, Joo T (2011) J Am Chem Soc 133:2932
19. Hsieh CC, Jiang CM, Chou PT (2010) Acc Chem Res 43:1364
20. Li GY, Zhao GJ, Liu YH, Han KL, He GZ (2010) J Comput Chem 31:1759–1765
21. Klymchenko AS, Yushchenko DA, Mely Y (2007) J Photochem Photobiol A 192:93
22. Li JN, Pu M, Fang DC, Wei M, He J, Evans DE (2012) J Mol Struct 1015:106–111
23. Lin TY, Tang KC, Yang SH, Shen JY, Cheng YM, Pan HA, Chi Y, Chou PT (2012) J Phys Chem A 116:4438–4444
24. Jayabharathi J, Thanikachalam V, Jayamoorthy K (2012) Mol Biomol Spectrosc 89:168–176
25. Gui G, Lan Z, Thiel W (2012) J Am Chem Soc 134:1662–1672
26. Ando K, Hayashi S, Kato S (2011) Phys Chem Chem Phys 13:11118–11127
27. Moreno M, Douhal A, Guallar V, Lluch JM, Castono O, Frutos LM (2001) J Phys Chem A 105:3887–3893
28. Iijima T, Mouotake A, Shinohara Y, Sato T, Nishimura Y, Arai T (2010) J Phys Chem A 114:1603–1609
29. Seo J, Kim S, Park SY (2004) J Am Chem Soc 126:11154–11155
30. Coppo P, Duati M, Kozhevnikov UN, Hofstraat L (2005) Angew Chem Int Ed 44:1806–1810
31. Yang YJ, Lowry M, Schonalter CM, Fakayode SO, Escobedo JO, Xu XY, Zhang HT, Jensen TJ, Franczck FR, Warner IM, Strongin RM (2006) J Am Chem Soc 128:14081–14092
32. Kim S, Seo J, Juang HK, Kim JJ, Park SY (2005) Adv Mater 17:2077–2082
33. Chou TP, Martines MZ, Studer SL (1991) J Phys Chem 95:10306
34. Tomin VI, Oncul S, Smolarczyk G, Demchenko AP (2007) Chem Phys 342:126
35. Golan A, Bravaya KB, Kudirka R, Kostko O, Leone SR, Krylov AI, Ahmed M (2012) Nat Chem 4:323–329
36. Catalan J, Valle J, Palonar J, Diaz C, Paz JL (1999) J Phys Chem A 103:10921
37. Schafer A, Huber C, Ahrichs R (1994) J Chem Phys 100:5829
38. Han KL, Zhao GJ (2010) Hydorgen bonding and transfer in the excited state. Wiley, Chichester
39. Zhao GJ, Han KL (2012) Acc Chem Res 45:404–413
40. Zhao GJ, Han KL, Stang PJ (2009) J Chem Theory Comput 5:1955–1958
41. Zhao GJ, Hn KL (2007) J Chem Phys 127:024306
42. Zhao GJ, Han KL (2007) J Phys Chem A 111:9218–9223
43. Zhao GJ, Han KL (2009) J Phys Chem A 113:14329
44. Zhao GJ, Han KL (2007) ChemPhysChem 9:1842–1846
45. Zhao GJ, Liu JY, Zhou LC, Han KL (2007) J Phys Chem B 111:8940
46. Zhao GJ, Han KL (2008) J Comput Chem 29:2010
47. Zhao GJ, Chen RK, Sun M, Li GY, Liu J, Gao Y, Han KL, Yang X, Sun LC (2008) Chem Eur J 14:6935–6947
48. Chai S, Zhao GJ, Song P, Yang SQ, Liu JY, Han KL (2009) Phys Chem Chem Phys 11:4385
49. Xie L, Chen Y, Wu W, Guo H, Zhao J, Yu X (2012) Dyes Pigments 92:1361–1369
50. Fang H, Kim Y (2011) J Phys Chem B 115:15048–15058
51. Catalan J, Diaz C, Perez P, Paz JL (2006) J Phys Chem A 110:9116–9122
52. Serrano-Andres L, Merchan M (2006) Chem Phys Lett 418:569–575
53. Zhao GJ, Han KL (2008) Biophys J 94:38
54. Biemann L, Kovalenko SA, Kleinermanns K, Mahrwald R, Markert M, Improta R (2011) J Am Chem Soc 133:19664–19667